HHS Public Access

Author manuscript

Magn Reson Med. Author manuscript; available in PMC 2022 April 01.

Published in final edited form as:

Magn Reson Med. 2021 April ; 85(4): 2212–2220. doi:10.1002/mrm.28549.

B0 and B1 Inhomogeneities in the Liver at 1.5T and 3.0T

Nathan T Roberts, BS[1,4], **Louis A Hinshaw**[1], **Timothy J Colgan, PhD**[1], **Takanori Ii**[1,7], **Diego Hernando, PhD**[1,2], **Scott B Reeder, MD, PhD**[1,2,3,5,6]

[1]Department of Radiology, University of Wisconsin – Madison, Madison, WI, United States

[2]Department of Medical Physics, University of Wisconsin – Madison, Madison, WI, United States

[3]Department of Biomedical Engineering, University of Wisconsin – Madison, Madison, WI, United States

[4]Department of Electrical and Computer Engineering, University of Wisconsin – Madison, Madison, WI, United States

[5]Department of Medicine, University of Wisconsin – Madison, Madison, WI, United States

[6]Department of Emergency Medicine, University of Wisconsin – Madison, Madison, WI, United States

[7]Department of Radiology, University of Yamanashi, Yamanashi, Japan

Abstract

Purpose: The purpose of this work is to characterize the magnitude and variability of B0 and B1 inhomogeneities in the liver in large cohorts of patients at both 1.5T and 3.0T.

Methods: Volumetric B0 and B1 maps were acquired over the liver of patients presenting for routine abdominal MRI. Regions of interest were drawn in the nine Couinaud segments of the liver and the average value was recorded. Magnitude and variation of measured averages in each segment were reported across all patients.

Results: A total of 316 B0 maps and 314 B1 maps, acquired at 1.5T and 3.0T on a variety of GE Healthcare MRI systems in 630 unique exams, were identified, analyzed, and, in the interest of reproducible research, de-identified and made public. Measured B0 inhomogeneities ranged (5th-95th percentiles) from −31.7Hz to 164.0Hz for 3.0T (−14.5Hz to 81.3Hz at 1.5T), while measured B1 inhomogeneities (ratio of actual over prescribed flip angle) ranged from 0.59 to 1.13 for 3.0T (0.83 to 1.11 at 1.5T).

Conclusion: This study provides robust characterization of B0 and B1 inhomogeneities in the liver to guide the development of imaging applications and protocols. Field strength, bore diameter, and sex were determined to be statistically significant effects for both B0 and B1 uniformity. Typical clinical liver imaging at 3.0T should expect B0 inhomogeneities ranging from approximately −100Hz to 250Hz (−50Hz to 150Hz at 1.5T) and B1 inhomogeneities ranging from approximately 0.4 to 1.3 (0.7 to 1.2 at 1.5T).

Corresponding Author: Scott B. Reeder, M.D., Ph.D., 1111 Highland Ave, WIMR2, Room 2472, Madison, WI, 53705, USA. sreeder@wisc.edu.

Keywords

magnetic resonance imaging; liver; B0; B1; inhomogeneities; magnetic field; dielectric effect; quantitative imaging biomarkers

Introduction

Inhomogeneities in the static (B0) and transmitted (B1) magnetic fields lead to artifacts and image degradation in a variety of imaging applications. Such inhomogeneities are of particular importance for quantitative imaging applications. B0 inhomogeneities in the static magnetic field are known to diminish the accuracy of quantitative parameter mapping (1), lead to image distortion in both standard and diffusion weighted echo planar imaging (2,3), cause banding artifacts in balance steady state free precession imaging (4), and exacerbate fat-water swaps in chemical shift-encoded (CSE)-MRI (5). B1 inhomogeneities in the local transmitted magnetic field are known to degrade image quality and cause spatially varying errors in the transmitted flip angle (6–8). Flip angle errors can lead to significant inaccuracies for quantitative T1 mapping applications, including inversion recovery and variable flip angle acquisitions (9–12).

In the liver, spoiled gradient echo (SGRE) acquisitions are commonly used both qualitatively and quantitatively. SGRE is routinely employed for dynamic contrast enhanced MRI (DCE-MRI) of liver perfusion (13,14), and in CSE-MRI (15) to quantify proton density fat fraction (PDFF) as a biomarker of tissue fat concentration (16,17), R2* as a biomarker of tissue iron concentration (18,19), and T1 as an emerging biomarker of tissue fibrosis (20). While the short acquisition times of SGRE are well suited for abdominal imaging, these acquisitions are sensitive to both B0 field map inhomogeneities and B1 flip angle errors, particularly when using multiple flip angles (1,9,21).

Producing reliable images and accurate measurements requires that quantitative imaging methods account for, or correct for, B0 and B1 inhomogeneities. Some methods are designed to be robust to these inhomogeneities (e.g. adiabatic pulses are robust to B1 inhomogeneities (22)), while other methods recognize and account for the inhomogeneities (e.g. CSE-MRI measures and corrects for B0 field variations (1)). In order to engineer image acquisition and reconstruction solutions that work broadly and robustly in a large number of patients, it is essential to know the scope of B0 and B1 inhomogeneities expected in vivo. Therefore, the purpose of this work is to determine the magnitude and variability of B0 and B1 inhomogeneities, separately, in the liver at both 1.5T and 3.0T in large cohorts of patients.

Methods

Patient Cohorts

In two separate cohorts of patients, from two independent and chronologically separate quality assurance studies, B0 and B1 maps were acquired in patients presenting for routine clinical MRI exams for a wide range of routine clinical applications. Typical pathology of patients presenting for abdominal imaging includes cirrhosis, metastatic disease, focal liver lesions, diffuse liver disease, biliary disease, pancreatic masses, renal lesions, and

hepatocellular carcinoma. All acquisitions were performed using standard transmit/receive system coils. Product prescan was performed prior to each acquisition. This algorithm uses the center slice of the prescribed volume to determine center frequency and linear B0 shim, for both 1.5T and 3.0T. On 3.0T systems equipped with dual RF transmit systems (see Table 1 for configurations), B1 amplitude and phase for the in-phase and quadrature channels were fixed to system specific vendor-specified values designed to optimize B1 uniformity in the liver. Data were analyzed retrospectively in a HIPAA compliant manner after approval from the local IRB.

B0 Acquisition and Analysis

3D B0 maps were acquired using a commercially available version of a quantitative CSE-MRI method (IDEAL IQ, GE Healthcare, Waukesha, WI) (23) on a variety of 1.5T and 3.0T clinical MRI systems (Table 1). IDEAL IQ is a vendor-specific implementation of CSE-MRI that acquires data using a multi-echo SGRE pulse sequence and estimates tissue parameter maps (including B0 field map) using a least squares fitting algorithm with T2* correction (24–26), as well as a region growing algorithm to avoid fat-water swaps (27); typical implementations of this reconstruction can be seen in (25,28–30). B0 maps were acquired with the following parameters: 42×42cm^2 FOV, 8mm slice thickness, 32 slices, 3^o prescribed flip angle, 128×128 matrix size, ±83.33kHz receiver bandwidth, with 6 echoes. At 1.5T, all echoes (TE1=0.9ms, ΔTE=1.48ms) were acquired in a single TR (9.5ms) in a single 17s breath-hold. To maintain optimal echo time spacing (30) at 3.0T, echoes were acquired in 2 shots of 3 echoes per TR (5.95ms) for a total of 6 echoes (TE1=0.8ms, ΔTE=1.65ms) in a single 16s breath-hold.

B0 field map values were measured in regions-of-interest (ROIs) placed in each of the nine Couinaud segments of the liver in the acquired field maps by an image analyst (primary reader, mentored by a senior radiologist with 20 years of experience), according to a standardized method proposed by Campo et al (31). ROIs were placed on the water image first, avoiding large blood vessels and bile ducts, and any obvious liver lesions or artifacts, and copied / pasted to the corresponding B0 maps. B0 field maps with fat-water swaps observed in the liver were screened from the study. B0 field map values (denoted ψ [Hz], relative to the center frequency) are related to changes in the static magnetic field (denoted ΔB0 [T]) by the Larmor equation $\psi = \gamma \Delta B0/2\pi$, where γ is the gyromagnetic ratio of ^{1}H.

B1 Acquisition and Analysis

2D interleaved B1 maps were acquired using a commercially available version of the Bloch-Siegert method (GE Healthcare, Waukesha, WI) (10) on a variety of 1.5T and 3.0T clinical MRI systems (Table 1) with the following parameters: 44×44cm^2 FOV, 10/10mm slice thickness/gap, 8 slices (spanning the entire liver), 15^o prescribed flip angle, 64×64 matrix size, ±15.63kHz receiver bandwidth, using an 8ms Fermi excitation pulse. At 1.5T, images were acquired in two 11s breath-holds with a 19ms TR and 12.4ms TE. At 3.0T, images were acquired in two 15s breath-holds with a 30ms TR and 12.2ms TE.

B1 map values (denoted β or B1 calibration coefficient) relate the measured transmitted flip angle (α_T) to prescribed flip angle (α_P) by the equation $\alpha_T = \beta\alpha_P$. β values were measured in

ROIs placed in each of the nine Couinaud segments of the liver in acquired β maps, in a manner similar to that performed for B0 map analysis (31).

Statistical Measurements

For both B0 and B1 measurements, two linear mixed models (32,33) were used to predict the B0 and B1 inhomogeneities as a function of field strength, bore diameter, sex, BMI and age. The first model controlled for non-uniform baselines stemming from Couinaud segment, patient, and MR technology (vendor model) differences by including all three factors in the model as random effects. By controlling for MR technology, the first model made bore diameter a redundant variable and it was therefore omitted. The second model controlled for both Couinaud segment and patient differences, but not MR technology in order to determine the effect and significance of bore diameter. Standardized parameters were obtained by fitting the model on a standardized version of the dataset. Effect sizes were labelled following Funder's recommendations (34). Datasets with incomplete/missing information (sex, BMI, or age) were not included in the linear mixed model.

To determine inter- and intra- reader reliability, 50 patient datasets from each B0 and B1 cohort were randomly selected to undergo two sets of repeated measurements, one repeated analysis by the aforementioned primary reader another unique analysis by a radiology resident acting as the secondary reader. Observer reliability was determined by interclass correlation coefficient (ICC), calculated for each Couinaud segment (35,36). ICC estimates and their 95% confident intervals were calculated in Python (37) using the DescTools package (38) from R (33). Inter-rater ICC was based on a single-rating, absolute-agreement, two-way random effects model. Intra-rater ICC was based on a single-rating, absolute-agreement, two-way mixed effects model.

Results

Patient Cohorts

Collectively, 630 maps (B0 and B1) were acquired on 6 different models and 10 total MR systems (See Table 1), in a total of 630 unique patients. In the interest of reproducible research, the set of anonymized B0 and B1 volumetric data that support the findings of this study are openly available in [repository name e.g. "figshare"] at http://doi.org/[doi], reference number [reference number]. [Note to reviewers and editors – data would be made available prior to publication of the manuscript, and this section will be updated].

B0 Acquisition and Analysis

B0 maps were acquired in 316 patients (166 females, 149 males) on both 1.5T (150 patients, 71 females, 78 males) and 3.0T (166 patients, 95 females, 71 males) clinical MRI systems. Examples of acquired B0 maps are shown in Figure 1. Patient age ranged from 7–88 years with a median age of 58.5 years. In 313 of the 316 patients where weight and height were recorded in the medical record, BMI ranged from 15.7–54.9 kg/m^2 with a median BMI of 29.4 kg/m^2.

Quartile and range statistics of field map measurements (Hz) for each segment across all patients are shown in Figure 2 (see also Supporting Information Figure S1). B0 measurements ranged from a 5th percentile of −14.5Hz to a 95th percentile of 81.3Hz for 1.5T and −31.7Hz to 164.0Hz for 3.0T.

Three patient datasets were excluded from the linear mixed model analysis due to missing BMI and sex information, leaving 313 total patient datasets (165 Female / 148 Male) from both 1.5T (147 datasets, 3 systems, 2 vendor models) and 3.0T (166 datasets, 5 systems, 3 vendor models) to be included in the linear mixed model (see Supporting Information Table S1). The first linear mixed model's total explanatory power is substantial (conditional R^2 = 0.80, marginal R^2=0.06). The model's intercept, corresponding to B0 = 0Hz, field strength = 1.5T, sex = Female, BMI = 21.7 kg/m^2, and age = 58.5, is at 27Hz (SE = 12.0Hz, $p < .05$). Within this model, the effect of field strength, 1.5T to 3.0T, is positive (medium and significant). The effect of sex, female to male, is positive (very small and significant). The effects of both BMI and age can be considered as tiny and not significant. A table with fitted coefficients, standard errors (SE), and p-values is included in Supporting Information Table S2. Figure 2 also shows the effect of bore diameter on B0 inhomogeneity, which was shown to be statistically significant (p=0.0056) in the second linear mixed model, with an average difference of 19.1Hz from increasing bore diameter from 60cm to 70cm (results from this linear mixed model are included in Supporting Information Table S3).

A total of 50 B0 patient datasets (23 at 1.5T, 27 at 3.0T) underwent repeated ROI analysis, in order to determine intra- and inter-reader variability. The median ICC estimates and 95% confidence intervals (CI) across segments were calculated to be 0.85 (good reliability) with 95% CI [0.75, 0.91] (good-excellent reliability) for inter-rater reliability and 0.92 (excellent reliability) with 95% CI [0.86,0.95] (good-excellent reliability) for intra-rater reliability. Supporting Information Figure S3 plots the ICC values per Couinaud segment and as a function of field strength.

B1 Acquisition and Analysis

B1 maps were acquired in 314 patients (169 females, 145 males) on both 1.5T (134 patients, 71 females, 63 males) and 3.0T (180 patients, 98 females, 82 males) clinical MRI systems. Examples of acquired B1 maps (β calibration coefficient maps) are shown in Figure 3. Patient age ranged from 17–95 years with a median age of 60 years. In 257 of the 314 patients where weight and height were recorded in the medical record, BMI ranged from 15.2–58.8 kg/m^2 with a median BMI of 29.3 kg/m^2.

Quartile and range statistics of B1 calibration coefficient measurements (β) for each segment across all patients are shown in Figure 4 (see also Supporting Information Figure S2). B1 measurements ranged from a 5th percentile of 0.83 to a 95th percentile of 1.11 for 1.5T and 0.59 to 1.13 for 3.0T.

Fifty-seven patient datasets were excluded from the linear mixed model analysis due to missing BMI information (which included the only 5 datasets acquired on a 3.0T system without dual RF drive), leaving 257 total patient datasets (145 Female / 112 Male) from both 1.5T (129 datasets, 3 systems, 2 vendor models) and 3.0T (128 datasets, 2 systems, 2 vendor

models) to be included in the linear mixed model (see Supporting Information Table S4). The first linear mixed model's total explanatory power is substantial (conditional $R^2 = 0.76$, marginal $R^2=0.17$). The model's intercept, corresponding to B1 (β)=1.0, field strength=1.5T, sex=Female, BMI=21.7 kg/m^2, and age= 60, is at 1.02 (SE = 0.05, p = 0.694). Within this model, the effect of field strength, 1.5T to 3.0T, is negative (large and significant). The effect of sex, female to male, is negative (medium and significant). The effect of BMI is negative (tiny and not significant). The effect of age is positive (very small and significant). A table with fitted coefficients, standard errors (SE), and p-values is included in Supporting Information Table S5. Figure 4 also shows the effect of bore diameter on B1 inhomogeneity, which was shown to be statistically significant ($p<<0.05$) in the second linear mixed model, with an average difference of −0.14 from increasing bore diameter from 60cm to 70cm (results from this linear mixed model are included in Supporting Information Table S6).

A total of 50 B1 patient datasets (17 at 1.5T, 33 at 3.0T) underwent repeated ROI analysis in order to determine intra- and inter-reader variability. The median ICC estimates and 95% confidence intervals across segments were calculated to be 0.85 (good reliability) with 95% CI [0.75, 0.91] (good-excellent reliability) for inter-rater reliability and 0.85 (good reliability) with 95% CI [0.75,0.91] (good-excellent reliability) for intra-rater reliability. Supporting Information Figure S3 plots the ICC values per Couinaud segment and as a function of field strength.

Discussion

B0 and B1 inhomogeneities are important confounders that impact many MR applications in the liver including both qualitative and quantitative MRI methods. In this work we successfully characterized the magnitude and variability of both B0 and B1 inhomogeneity in the liver at 1.5T and 3.0T, in a cohort of 630 unique patients.

Both B0 and B1 inhomogeneities were shown to exhibit higher magnitude and variability in the liver at 3.0T compared with 1.5T. At both field strengths, we noted relatively higher magnitude and variability of B0 inhomogeneities in segments 4a, 4b, 7, and 8 when compared to other segments. These segments are in closer proximity to the lung bases (4a, 7, 8) and transverse colon (4b), which may explain these observations. We also observed that more severe B1 inhomogeneities were experienced in the lateral segment of the left lobe of the liver (segments II and III), where shading artifacts related to B1 inhomogeneities are most commonly observed (39,40).

Mixed linear model analysis revealed that after field strength effects, sex was a more significant cause of variation for both B0 and B1 inhomogeneities than both BMI and age. This observation may be explained by the geometry of the liver with respect to female breast tissue. BMI, which we expected to have a larger effect, was not statistically significant in either B0 or B1 measurements. In 3.0T acquisitions, increasing bore diameter (which may also affect patient positioning) was shown to be a statistically significant effect adversely affecting both B0 and B1 uniformity. More generally, the first linear mixed model analysis controlled for vendor model differences (encompassing bore diameter) that may contribute

to baseline shifts in B0 and B1 measurements. Plots showing these baseline shifts are included in Supporting Information Figures S1 and S2.

Understanding the range of expected B0 and B1 inhomogeneities experienced in vivo is a necessary first step prior to developing engineering solutions aimed at avoiding or correcting for these confounders. This characterization can also be used to optimize protocols aimed at minimizing the effects of B0 and B1 inhomogeneities (e.g. spatial resolution in echo planar imaging and optimization of CSE-MRI acquisition parameters, like echo times, in fat-water imaging). Further, this work may also assist vendors who are developing hardware engineering solutions to reduce B0 and B1 inhomogeneities. Finally, knowing the effect of field strength on these confounders may help guide the translation of applications between field strengths during technical development or protocol optimization. This work provides this characterization in the liver for 1.5T and 3.0T, with two limitations. First, signal-to-noise ratio differences between field strengths were not explicitly controlled in the B0 and B1 acquisition protocols; however, any potential confounding effect of spatial variance on the reported results should be eliminated by the averaging of ROIs during the analysis. Second, of the 346 acquisitions on 3.0T MR systems, all but 5 (which were excluded from the B1 analysis) used dual RF transmission which generally improves B1 homogeneity (41). Future investigations would be required to characterize these inhomogeneities on 3.0T systems with single-coil RF transmission.

Although MR systems were limited to a single vendor, this work provides data from a large cohort of patients, which can be reliably used to guide future MR application development for liver imaging. Future studies should confirm these results across multiple vendor platforms. Finally, this study was limited to broad descriptive variables including age, sex, and BMI in the linear mixed model analysis. Other variables, such as body composition analysis derived from segmented 3D datasets (42), could reveal new and important information about the effect of patient abdominal geometry on B0 and B1 homogeneity.

In summary, this study provides robust characterization of B0 and B1 inhomogeneities in the liver, as measured in two large cohorts of patients at both 1.5T and 3.0T. All summary results from this study, as well as the original B0 and B1 maps have been made available online, in the interests of reproducible research, and to assist researchers who are developing engineering solutions needed to address the confounding effects of B0 and B1 inhomogeneities in the abdomen.

Supplementary Material

Refer to Web version on PubMed Central for supplementary material.

Acknowledgements

The authors wish to thank Dr. David Harris, for his assistance with manuscript preparation, and Kyle Davis, for his assistance with statistical modeling. This work was supported by the NIH (R01-DK117354, R01-DK100651, K24-DK102595, and R01-DK088925). The authors also acknowledge GE Healthcare who provides research support to the University of Wisconsin-Madison. Finally, Dr. Reeder is a Romnes Faculty Fellow, and has received an award provided by the University of Wisconsin-Madison Office of the Vice Chancellor for Research and Graduate Education with funding from the Wisconsin Alumni Research Foundation.

References

1. Hernando D, Vigen KK, Shimakawa A, Reeder SB. R*(2) mapping in the presence of macroscopic B(0) field variations. Magn. Reson. Med 2012;68:830–40 doi: 10.1002/mrm.23306. [PubMed: 22161866]
2. Jezzard P, Balaban RS. Correction for geometric distortion in echo planar images from B0 field variations. Magn. Reson. Med 1995;34:65–73 doi: 10.1002/mrm.1910340111. [PubMed: 7674900]
3. Reese TG, Heid O, Weisskoff RM, Wedeen VJ. Reduction of eddy-current-induced distortion in diffusion MRI using a twice-refocused spin echo. Magn. Reson. Med 2003;49:177–82 doi: 10.1002/mrm.10308. [PubMed: 12509835]
4. Quist B, Hargreaves BA, Daniel BL, Saranathan M. Balanced SSFP Dixon Imaging with Banding-Artifact Reduction at 3T. Magn. Reson. Med 2015;74:706–715 doi: 10.1002/mrm.25449. [PubMed: 25227766]
5. Hernando D, Haldar JP, Sutton BP, Ma J, Kellman P, Liang ZP. Joint estimation of water/fat images and field inhomogeneity map. Magn Reson Med 2008;59:571–80 doi: 10.1002/mrm.21522. [PubMed: 18306409]
6. Ibrahim TS, Lee R, Abduljalil AM, Baertlein BA, Robitaille PM. Dielectric resonances and B(1) field inhomogeneity in UHFMRI: computational analysis and experimental findings. Magn. Reson. Imaging 2001;19:219–26. [PubMed: 11358660]
7. Yang QX, Wang J, Zhang X, et al. Analysis of wave behavior in lossy dielectric samples at high field. Magn. Reson. Med 2002;47:982–9 doi: 10.1002/mrm.10137. [PubMed: 11979578]
8. Collins CM, Liu W, Schreiber W, Yang QX, Smith MB. Central brightening due to constructive interference with, without, and despite dielectric resonance. J Magn Reson Imaging 2005;21:192–6 doi: 10.1002/jmri.20245. [PubMed: 15666397]
9. Deoni SC. Correction of main and transmit magnetic field (B0 and B1) inhomogeneity effects in multicomponent-driven equilibrium single-pulse observation of T1 and T2. Magn Reson Med 2011;65:1021–35 doi: 10.1002/mrm.22685. [PubMed: 21413066]
10. Sacolick LI, Wiesinger F, Hancu I, Vogel MW. B1 mapping by Bloch-Siegert shift. Magn. Reson. Med 2010;63:1315–1322 doi: 10.1002/mrm.22357. [PubMed: 20432302]
11. Warntjes JB, Dahlqvist O, Lundberg P. Novel method for rapid, simultaneous T1, T2*, and proton density quantification. Magn. Reson. Med 2007;57:528–37 doi: 10.1002/mrm.21165. [PubMed: 17326183]
12. Saekho S, Yip C, Noll DC, Boada FE, Stenger VA. Fast-kz three-dimensional tailored radiofrequency pulse for reduced B1 inhomogeneity. Magn. Reson. Med 2006;55:719–724 doi: 10.1002/mrm.20840. [PubMed: 16526012]
13. Pandharipande PV, Krinsky GA, Rusinek H, Lee VS. Perfusion imaging of the liver: current challenges and future goals. Radiology 2005;234:661–73 doi: 10.1148/radiol.2343031362. [PubMed: 15734925]
14. Do RK, Rusinek H, Taouli B. Dynamic contrast-enhanced MR imaging of the liver: current status and future directions. Magn. Reson. Imaging Clin. N. Am 2009;17:339–49 doi: 10.1016/j.mric.2009.01.009. [PubMed: 19406362]
15. Liu CY, McKenzie CA, Yu H, Brittain JH, Reeder SB. Fat quantification with IDEAL gradient echo imaging: correction of bias from T(1) and noise. Magn Reson Med 2007;58:354–64 doi: 10.1002/mrm.21301. [PubMed: 17654578]
16. Reeder SB, Cruite I, Hamilton G, Sirlin CB. Quantitative Assessment of Liver Fat with Magnetic Resonance Imaging and Spectroscopy. J Magn Reson Imaging 2011;34:spcone doi: 10.1002/jmri.22775.
17. Reeder SB, Hu HH, Sirlin CB. Proton density fat-fraction: a standardized MR-based biomarker of tissue fat concentration. J Magn Reson Imaging 2012;36:1011–4 doi: 10.1002/jmri.23741. [PubMed: 22777847]
18. Hernando D, Levin YS, Sirlin CB, Reeder SB. Quantification of liver iron with MRI: state of the art and remaining challenges. J Magn Reson Imaging 2014;40:1003–21 doi: 10.1002/jmri.24584. [PubMed: 24585403]

19. Sirlin CB, Reeder SB. Magnetic resonance imaging quantification of liver iron. Magn. Reson. Imaging Clin. N. Am 2010;18:359–81, ix doi: 10.1016/j.mric.2010.08.014. [PubMed: 21094445]
20. Banerjee R, Pavlides M, Tunnicliffe EM, et al. Multiparametric magnetic resonance for the non-invasive diagnosis of liver disease. J Hepatol 2014;60:69–77 doi: 10.1016/j.jhep.2013.09.002. [PubMed: 24036007]
21. Cheng H-LM, Wright GA. Rapid high-resolution T1 mapping by variable flip angles: Accurate and precise measurements in the presence of radiofrequency field inhomogeneity. Magn. Reson. Med 2006;55:566–574 doi: 10.1002/mrm.20791. [PubMed: 16450365]
22. De Graaf RA, Nicolay K. Adiabatic rf pulses: Applications to in vivo NMR. Concepts Magn. Reson 1997;9:247–268 doi: 10.1002/(sici)1099-0534(1997)9:4<247::aid-cmr4>3.0.co;2-z.
23. Reeder SB, Wen Z, Yu H, et al. Multicoil Dixon chemical species separation with an iterative least-squares estimation method. Magn Reson Med 2004;51:35–45 doi: 10.1002/mrm.10675. [PubMed: 14705043]
24. Reeder SB, Pineda AR, Wen Z, et al. Iterative decomposition of water and fat with echo asymmetry and least-squares estimation (IDEAL): application with fast spin-echo imaging. Magn. Reson. Med 2005;54:636–644 doi: 10.1002/mrm.20624. [PubMed: 16092103]
25. Yu H, McKenzie CA, Shimakawa A, et al. Multiecho reconstruction for simultaneous water-fat decomposition and T2* estimation. J Magn Reson Imaging 2007;26:1153–61 doi: 10.1002/jmri.21090. [PubMed: 17896369]
26. Yu H, Shimakawa A, McKenzie CA, Brodsky E, Brittain JH, Reeder SB. Multiecho water-fat separation and simultaneous R2* estimation with multifrequency fat spectrum modeling. Magn. Reson. Med 2008;60:1122–1134 doi: 10.1002/mrm.21737. [PubMed: 18956464]
27. Yu H, Reeder SB, Shimakawa A, Brittain JH, Pelc NJ. Field map estimation with a region growing scheme for iterative 3-point water-fat decomposition. Magn. Reson. Med 2005;54:1032–1039 doi: 10.1002/mrm.20654. [PubMed: 16142718]
28. Meisamy S, Hines CDG, Hamilton G, et al. Quantification of hepatic steatosis with T1-independent, T2-corrected MR imaging with spectral modeling of fat: blinded comparison with MR spectroscopy. Radiology 2011;258:767–775 doi: 10.1148/radiol.10100708. [PubMed: 21248233]
29. Hines CDG, Frydrychowicz A, Hamilton G, et al. T(1) independent, T(2) (*) corrected chemical shift based fat-water separation with multi-peak fat spectral modeling is an accurate and precise measure of hepatic steatosis. J. Magn. Reson. Imaging JMRI 2011;33:873–881 doi: 10.1002/jmri.22514. [PubMed: 21448952]
30. Hernando D, Hines CD, Yu H, Reeder SB. Addressing phase errors in fat-water imaging using a mixed magnitude/complex fitting method. Magn Reson Med 2012;67:638–44 doi: 10.1002/mrm.23044. [PubMed: 21713978]
31. Campo CA, Hernando D, Schubert T, Bookwalter CA, Pay AJV, Reeder SB. Standardized Approach for ROI-Based Measurements of Proton Density Fat Fraction and R2* in the Liver. Am. J. Roentgenol 2017;209:592–603 doi: 10.2214/AJR.17.17812. [PubMed: 28705058]
32. Bates D, Mächler M, Bolker B, Walker S. Fitting Linear Mixed-Effects Models Using lme4. J. Stat. Softw 2015;67:1–48 doi: 10.18637/jss.v067.i01.
33. R Core Team. R: A language and environment for statistical computing. Vienna, Austria: R Foundation for Statistical Computing; 2019.
34. Funder DC, Ozer DJ. Evaluating Effect Size in Psychological Research: Sense and Nonsense: Adv. Methods Pract. Psychol. Sci 2019 doi: 10.1177/2515245919847202.
35. Koo TK, Li MY. A Guideline of Selecting and Reporting Intraclass Correlation Coefficients for Reliability Research. J. Chiropr. Med 2016;15:155–163 doi: 10.1016/j.jcm.2016.02.012. [PubMed: 27330520]
36. Popović ZB, Thomas JD. Assessing observer variability: a user's guide. Cardiovasc. Diagn. Ther 2017;7:317–324 doi: 10.21037/cdt.2017.03.12. [PubMed: 28567357]
37. Python Programming Language. Python Software Foundation.
38. Signorell A, et mult. al. DescTools: Tools for descriptive statistics; 2020.
39. Bernstein MA, Huston J, Ward HA. Imaging artifacts at 3.0T. J. Magn. Reson. Imaging 2006;24:735–746 doi: 10.1002/jmri.20698. [PubMed: 16958057]

40. Andrews T, Ghostine J, Gonyea J, Ebert G, Braff S, Filippi C. Reduction in dielectric shading in liver on clinical 3T parallel transmission MR system. In: ; 2010.

41. Brink WM, Gulani V, Webb AG. Clinical applications of dual-channel transmit MRI: A review: Clinical Applications of Dual-Channel Transmit MRI. J. Magn. Reson. Imaging 2015;42:855–869 doi: 10.1002/jmri.24791. [PubMed: 25854179]

42. Borga M, West J, Bell JD, et al. Advanced body composition assessment: from body mass index to body composition profiling. J. Investig. Med. Off. Publ. Am. Fed. Clin. Res 2018;66:1–9 doi: 10.1136/jim-2018-000722.

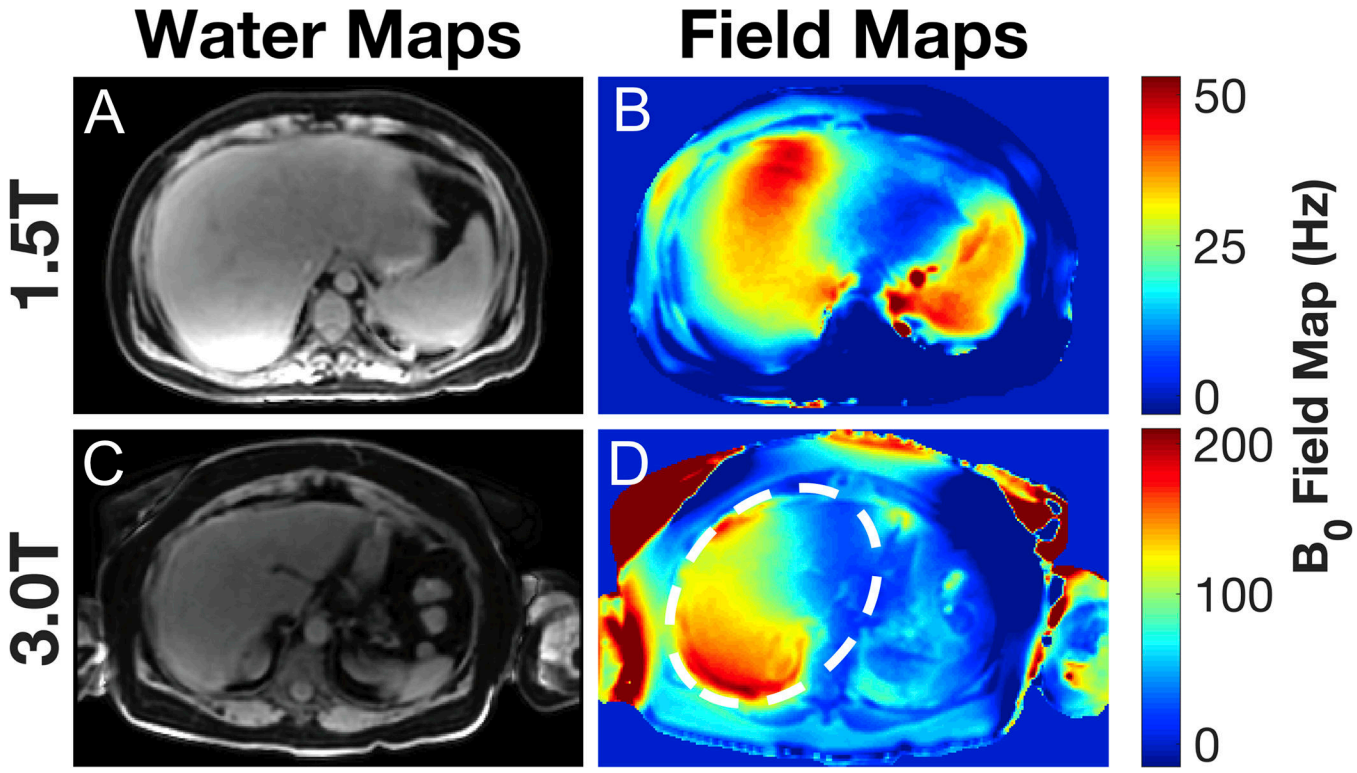

Figure 1.

B0 field map inhomogeneities vary spatially across the liver and tend to increase with field strength. Note the pronounced difference between the 1.5T and 3.0T field map color scales and the variability within a single liver at 3.0T (D, dashed oval). Examples from both field strengths of IDEAL IQ B0 field maps (B,D) are shown above with their accompanying water maps (A,C). Note that field map values (denoted ψ [Hz]) are related to changes in the static magnetic field (denoted $\Delta B0$ [T]) by the Larmor equation $\psi = \gamma \Delta B0/2\pi$, where γ is the gyromagnetic ratio of ^{1}H.

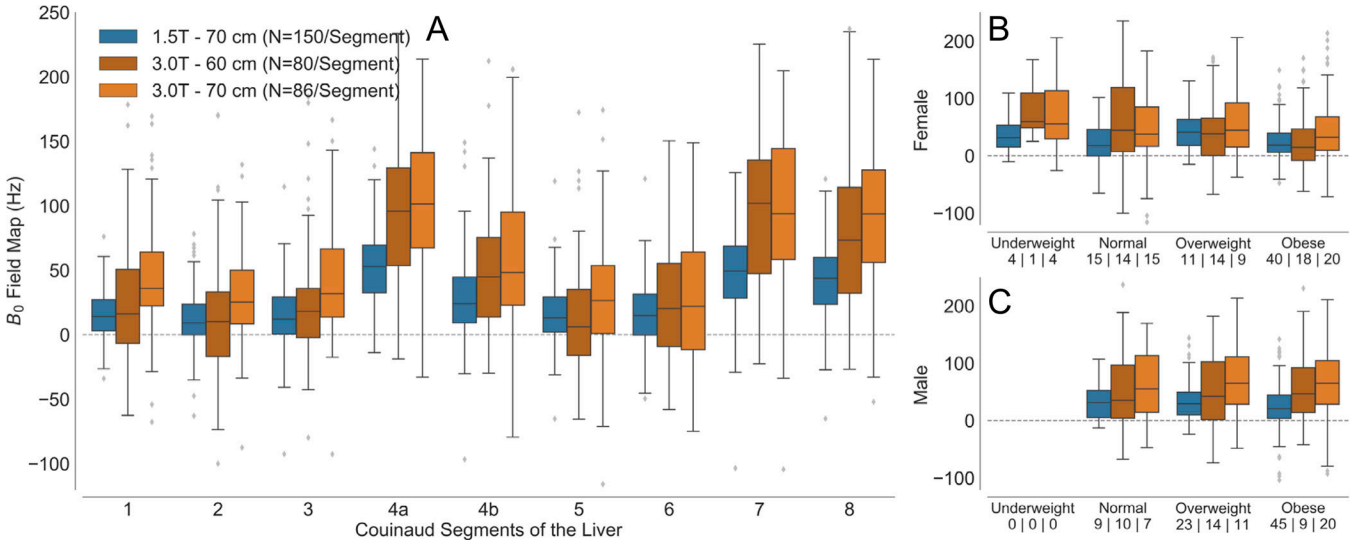

Figure 2.

Field map errors exhibit greater magnitude and variability in the liver at 3.0T than at 1.5T, however, they are present in all segments of the human liver. In 3.0T acquisitions, bore diameter was observed to be a small yet statistically significant factor contributing to B0 inhomogeneity. Quartile and range statistics (with statistical outliers shown in gray) of field map measurements (Hz) are plotted across segments (A), across BMI in females (B), and across BMI in males (C). BMI was defined as: underweight (<18.5kg/m^2), normal (<25kg/m^2), overweight (<30kg/m^2) and obese (≥30kg/m^2). Numerical values under each BMI x-axis label give the number of patients included in the statistics for 1.5T − 70cm bore, 3.0T − 60cm bore, and 3.0T − 70cm bore, respectively. Note that field map values (denoted ψ [Hz]) are related to changes in the static magnetic field (denoted $\Delta B0$ [T]) by the Larmor equation $\psi = \gamma \Delta B0$, where γ is the gyromagnetic ratio of ^1H.

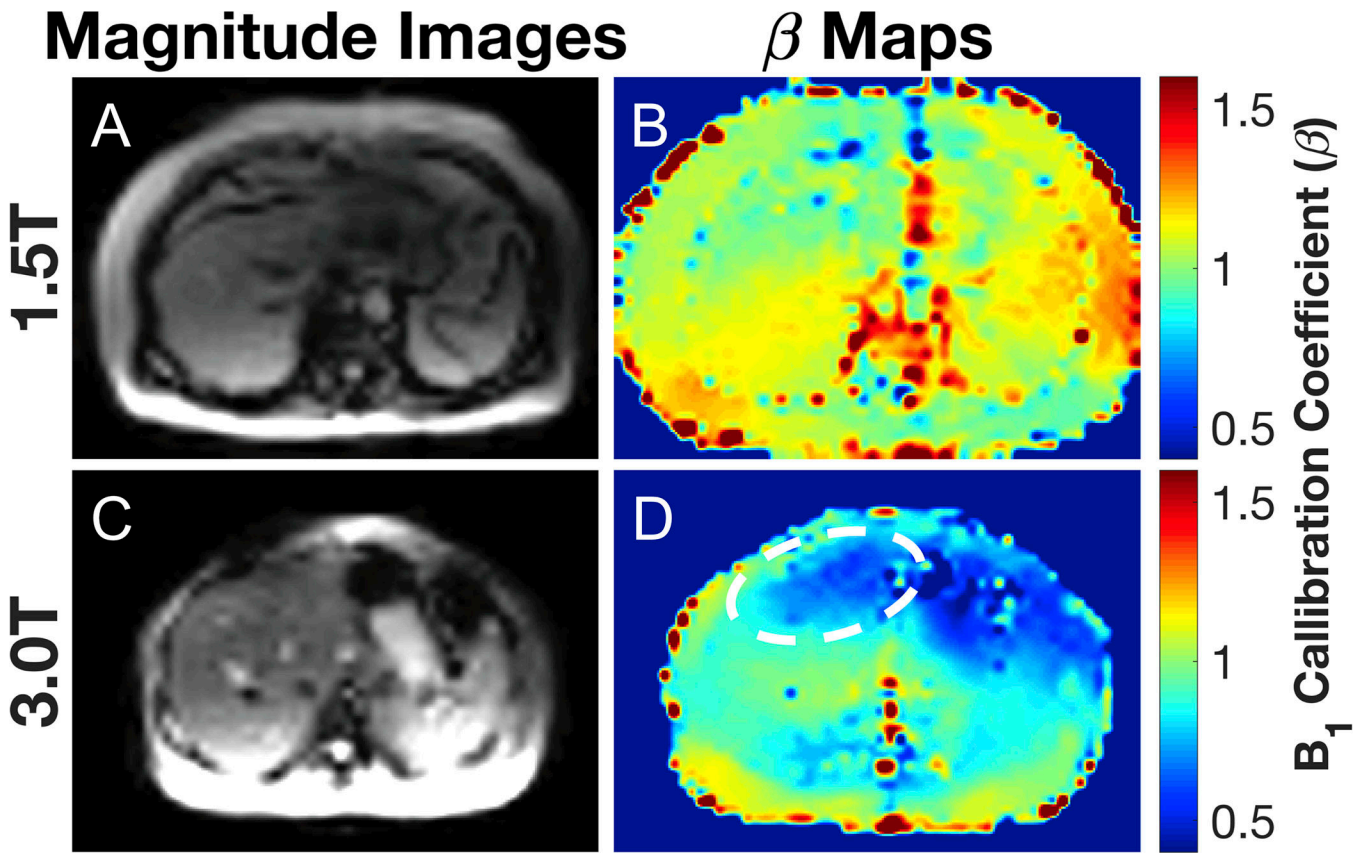

Figure 3.

Flip angle (B1) errors vary spatially across the liver. Note the large B1 inhomogeneities in segments II/III of the 3.0T example (D, dashed oval). Examples from both field strengths of Bloch-Siegert B1 calibration coefficient maps (B,D) are shown above with their accompanying magnitude gradient echo images (A,C). Note that transmitted flip angle (α_T) is related to prescribed flip angle (α_P) by the equation $\alpha_T=\beta\alpha_P$.

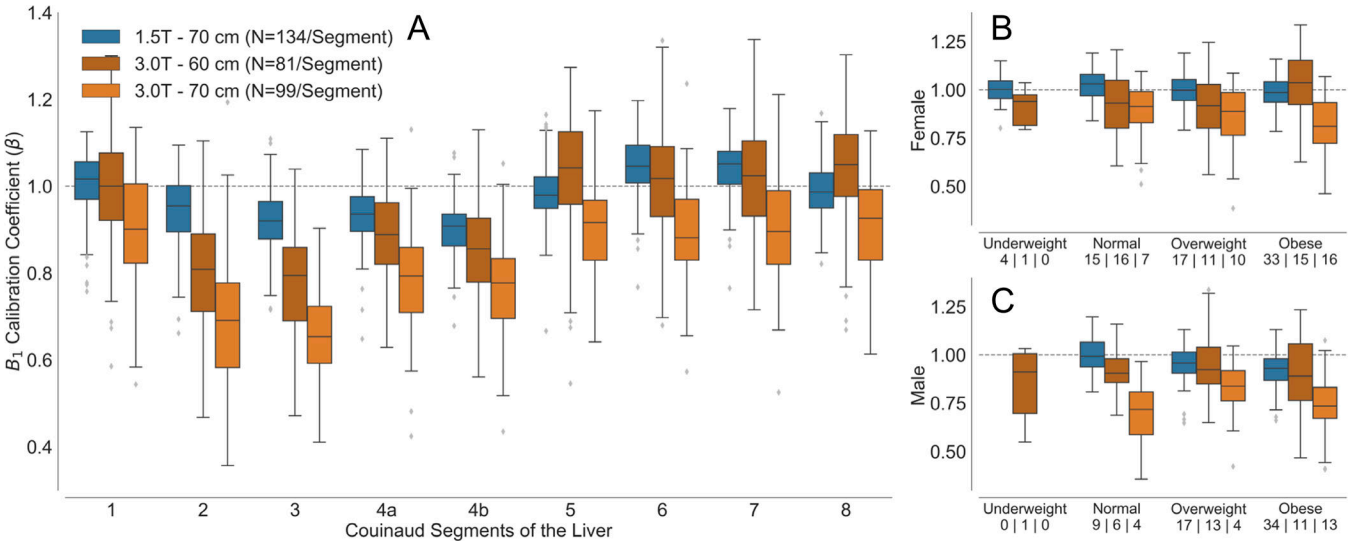

Figure 4.

B1 inhomogeneities are present in the liver at both 1.5T and 3.0T, with flip angle errors in 3.0T acquisitions exhibiting larger magnitude and variability. In 3.0T acquisitions, bore diameter was observed to be a very large and statistically significant factor contributing to B1 inhomogeneity. Of particular note are the average B1 inhomogeneities (β) in the lateral segment of the left lobe of the liver (segments II and III) at 3.0T which manifest the largest average flip angle errors. Quartile and range statistics (with statistical outliers shown in gray) of B1 inhomogeneity measurements are plotted across segments (A), across BMI in females (B), and across BMI in males (C). BMI was defined as: underweight (<18.5kg/m^2), normal (<25kg/m^2), overweight (<30kg/m^2) and obese (≥30kg/m^2). Numerical values under each BMI x-axis label give the number of patients included in the statistics for 1.5T - 70cm bore, 3.0T - 60cm bore, and 3.0T - 70cm bore, respectively. Note that transmitted flip angle (αT) is related to prescribed flip angle (αP) by the equation αT=βαP.

Table 1.

B0 and B1 maps were acquired and analyzed in a total of 630 patients presenting for routine clinical abdominal MRI, on a variety of GE Healthcare MRI systems.

Cohort					
Acquisition	**Total Patients**	**Female / Male**	**1.5T / 3.0T**	**Median Age**	**Age Range**
B0	316	166 / 149	150 / 166	58.5	7–88
B1	314	169 / 145	134 / 180	60	17–95
MRI Systems					
1.5T (3)			**3.0T (7)**		
GEHC Optima MR450W (2)			*GEHC Discovery MR750W (2)		
GEHC Signa Artist			*GEHC Signa Premier (2)		
			**GEHC Discovery MR750 (2)		
			*GEHC Signa Architect		

*Equipped with dual RF transmit systems

**Only one of the Discovery MR750 systems is dual RF transmit